https://doi.org/10.5194/egusphere-2024-1499
Preprint. Discussion started: 1 July 2024


# Quantifying the Buttressing Contribution of Sea Ice to Crane Glacier

Richard Parsons[1], Sainan Sun[1], G. Hilmar Gudmundsson[1], Jan Wuite[2], and Thomas Nagler[2]

[1]Department of Geography and Environmental Sciences, Northumbria University, Newcastle upon Tyne, NE1 8ST, UK
[2]ENVEO IT GmbH, Fürstenweg 176, A-6020 Innsbruck, Austria

**Correspondence:** Richard Parsons (richard.parsons@northumbria.ac.uk)

**Abstract.** The January 2022 disintegration of landfast sea ice in the Larsen B Embayment was closely followed by a significant acceleration of ice flow and ice-front retreat of numerous outlet glaciers. Crane Glacier was a notable example of this, with 6 km of its floating ice shelf lost to calving in the first month following the sea ice disintegration and a 3.4% increase in terminus flow speeds over the same time period. In this study we quantify for the first time the buttressing resistance that the sea ice provided to Crane with ice-flow model Úa. We constrained our model with satellite derived elevation profiles of glacier, sea ice and associated melange downstream of Crane's terminus and reconstructed the observed flow velocities by optimising the rheology rate factor of both the glacier and sea ice allowing us to quantify the stress regime throughout our model domain. Results showed that resistive backstresses were imparted to Crane by the sea ice with a mean buttressing number of 0.68 calculated at the glacier terminus. In addition, diagnostic modelling showed an expected 19.2 kPa mean increase in extensional stress at the ice-front following the loss of buttressing sea ice. This perturbation in stress likely triggered the observed rapid calving over the near terminus region, leading to the loss of sections of Crane's buttressing floating ice shelf and further acceleration of ice flow in the subsequent months.

## 1 Introduction

Sea ice plays an important role in regulating the dynamic behaviour of ice shelves and outlet glaciers (Massom et al., 2010; Arthur et al., 2021; Christie et al., 2022). Until 2016, observations spanning almost four decades showed a gradually increasing trend in Antarctic sea ice extent (Fogt et al., 2022). Unprecedented annual decreases have however been seen since this time with new record lows set in February 2017, 2022 (Raphael and Handcock, 2022) and again in 2023 (Liu et al., 2023). This recent behavioural shift may indicate a new forward trend in decreasing sea ice extent (Purich and Doddridge, 2023) which in turn could impact upon the stability of adjoining ice shelves and outlet glaciers and increase rates of ice discharge into the ocean (Massom et al., 2018).

Resistive stresses directly imparted by sea ice at a glacier's terminus have not yet been assessed quantitatively. Whilst the buttressing capacity of ice shelves has been evaluated in numerous studies (Gudmundsson et al., 2023; Fürst et al., 2016; Reese et al., 2018), sea ice buttressing has so far only been discussed in terms of causal links between changes in ice flow velocity and perturbations in sea ice coverage. Examples of this include the seasonal acceleration of the Totton Ice Shelf (Greene et al.,

https://doi.org/10.5194/egusphere-2024-1499
Preprint. Discussion started: 1 July 2024


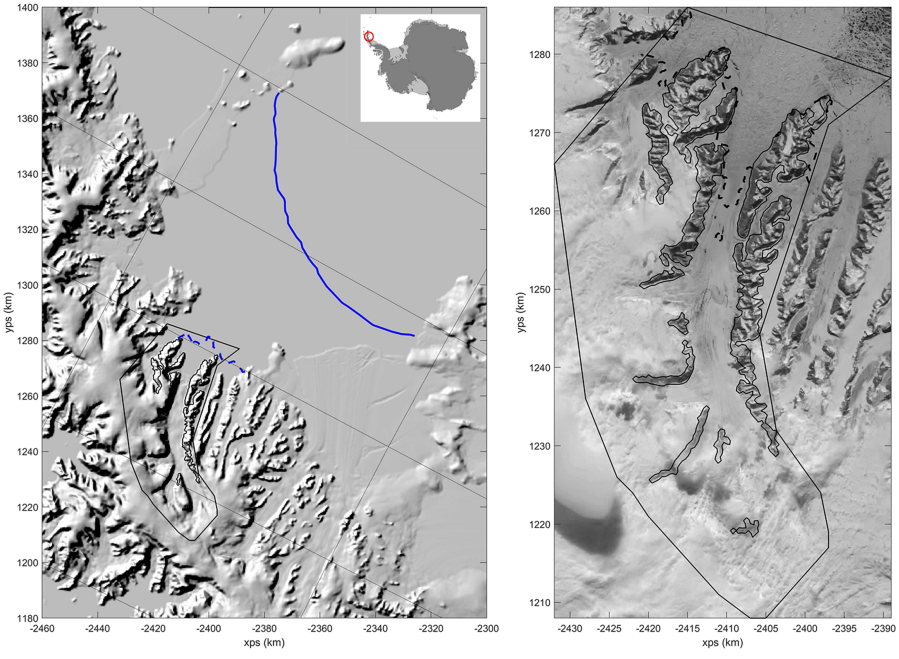


**Figure 1.** The left hand panel shows an overview of the Larsen B embayment displayed on a hill shaded relief map of the REMA mosaic for Antarctica (Howat et al., 2019), with the location of Larsen B highlighted by the red ring in the subset outline of Antarctica (source: BedMachine v3 (Morlighem, 2022)). The black line outlines the extent of the model domain. The solid blue line denotes the approximate extent of sea ice in the months prior to its disintegration and the blue dashed line shows the sea ice extent after disintegration with coordinates extracted from LandSat 8 imagery (24/02/2022). The right hand panel shows a close up view of Crane Glacier captured by LandSat 9 (13/12/2021). The dashed black line represents the grounding line location with the solid black line showing the extent of the model domain.

2018) and the Parker Ice tongue (Gomez-Fell et al., 2022). More recently, the 2022 widespread disintegration of sea ice in the Larsen B Embayment provided an opportunity to assess the impact of instantaneous sea ice loss to multiple glaciers, aided by the abundant present-day observational datasets for the region (Sun et al., 2023; Ochwat et al., 2024; Surawy-Stepney et al., 2024). Furthermore, the buttressing capacity of sea ice was brought in to question due to the similarities in the response of the regions outlet glaciers following this loss of sea ice and the 2002 collapse of the Larsen B Ice Shelf (Scambos et al., 2004; Rignot et al., 2004; De Rydt et al., 2015).

Following the 2002 ice-shelf collapse, Crane Glacier (Fig. 1) notably retreated by more than 10 km in just over two years (Needell and Holschuh, 2023) with ice flow across the grounding line increasing by up to three times over a similar period (Rignot et al., 2004). Crane's longer-term response was more complex and following the initial rapid retreat, phases of arrest and subsequent re-advance were exhibited (Needell and Holschuh, 2023; Rott et al., 2018; Wuite et al., 2015).

Sea ice formed seasonally in the Larsen B embayment each year following the 2002 ice-shelf collapse, but in 2011 the sea ice became landfast before further developing into thicker and more extensive multi-year ice (Ochwat et al., 2024; Surawy-

https://doi.org/10.5194/egusphere-2024-1499
Preprint. Discussion started: 1 July 2024


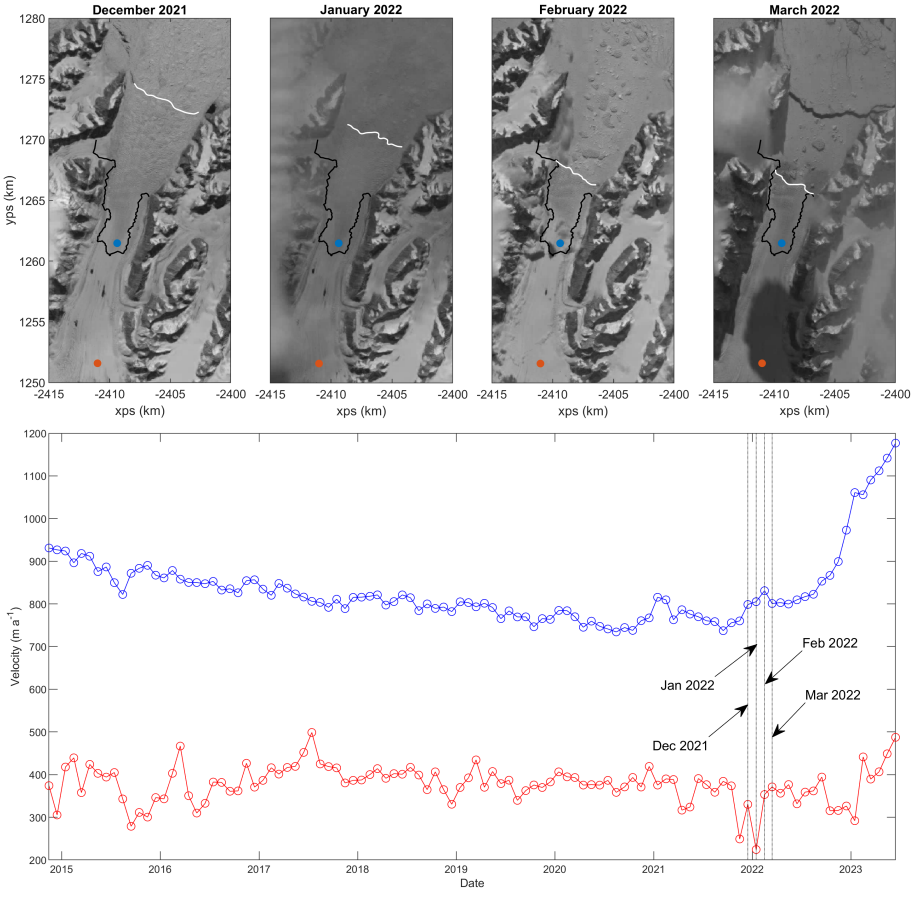


**Figure 2.** Top row: Close up views of Crane's outlet in Dec 2021 and Jan, Feb, Mar 2022, cropped from Landsat 8 and 9 satellite images, courtesy of U.S. Geological Survey (Table 1). The sea ice was still intact in December 2021 and a degree of sea ice remained in the outlet of the fjord in the months following the sea ice disintegration. The black line shows the modelled grounding line position and the white line shows the terminus location. The coloured dots are locations from which velocity data was extracted by ENVEO et al. (2021). Bottom row: Monthly averaged ice flow velocities from 2015-2023 (ENVEO et al., 2021). The blue and red lines represent the flow velocities at the corresponding blue and red location markers shown in the top row images with the black vertical lines corresponding to the dates of the figures above.

Stepney et al., 2024). The thickness of this sea ice was estimated to be between 2.5 m and 4 m across the embayment (Scambos et al., 2017), though thicknesses of magnitude of tens to hundreds of metres was reported for trapped melange elements close to the glacier outlets (Ochwat et al., 2024). The presence of fast ice seemingly aided a decade long re-advance of Crane, but the sea ice disintegration in mid-January 2022 triggered a second period of rapid retreat (Needell and Holschuh, 2023). Ice flow velocities were also affected with acceleration observed in the months following the disintegration, however a more significant increase in flow speeds over both grounded and floating ice was not observed until later in the year (Fig. 2, Movie S2).

https://doi.org/10.5194/egusphere-2024-1499
Preprint. Discussion started: 1 July 2024


The similarities between the 2002 and 2022 events led to multiple studies assessing the role that sea ice played in buttressing Larsen B's outlet glaciers, including, but not limited to, Crane glacier (Sun et al., 2023; Ochwat et al., 2024; Surawy-Stepney et al., 2024). However, conclusions on the buttressing capacity of sea ice from these studies varied. Sun et al. (2023) argued that whilst the sea ice covered the same area as the previously existing ice shelf, the buttressing backstresses were small as damage could more readily propagate through sea ice due to its weaker and thinner makeup, therefore limiting its resistive potential. This was evidenced by a lack of instantaneous acceleration at six glaciers following the disintegration and near-zero correlation between sea ice extent and glacier velocities (Sun et al., 2023). A delayed velocity response observed 8 months later was attributed to the retreat of Crane's ice front, rather than being directly due to the collapse of the sea ice (Sun et al., 2023). In contrast, Ochwat et al. (2024) recognised the similarities in dynamic response following the sea ice and ice shelf break-ups, including instantaneous acceleration of ice flow, to mean there were parallels in the buttressing resistance provided by the two different ice masses. The destabilisation and calving of floating ice tongues in different outlet glaciers in Larsen B were therefore attributed to the loss of sea ice buttressing (Ochwat et al., 2024). Surawy-Stepney et al. (2024) used an ice-sheet model to estimate the effect of sea ice on Larsen B glaciers. The authors first optimised the rate factor of the glaciers to reproduce the observed velocity field without sea ice, then artificially added sea ice with different thickness to calculate the resultant differences in ice-flow speed. The study concluded that whilst the sea ice affected the dynamic behaviour of floating ice in different glacier outlets, this was not a result of direct buttressing in the same context as is understood for ice shelves. Instead, any buttressing from sea ice coverage was attributed to secondary processes including ocean swell attenuation (Teder et al., 2022; Christie et al., 2022) and bonding of melange in areas downstream of glacier termini (Robel, 2017). The potential issue of this approach lies in the initialisation process: by solving the optimisation problem without including sea ice, the buttressing effect of sea ice, if any, has been compensated by adjusting the rate factor of the glacier.

Here we seek to quantify for the first time the buttressing resistance of sea ice to Crane Glacier using ice-sheet model Úa, with a computational domain including both the glacier and ambient sea ice. We quantify the buttressing contribution using the buttressing number (Schoof, 2007) and further assess the change in the near-terminus stress field following the sea ice disintegration, which may have triggered retreat of Crane's ice-front. Finally, we test the robustness of the ice-sheet model in determining the resistive stresses imparted by sea ice by investigating the sensitivity of our results to changes in the prescribed input thickness of sea ice. This is to improve confidence in employing our methodology in scenarios where uncertainty in sea ice thickness measurements is of concern.

## 2 Datasets

In order to configure a model geometry representative of Crane Glacier prior to the disintegration of sea ice in the Larsen B embayment, we utilised a range of REMA strip DEMs defined at 2 m spatial resolution (Howat et al., 2019) to create a continuous surface elevation profile across our model domain. The strips were timestamped between 30th September 2020 and 16th January 2022 with the most recent strip covering the near-terminus region and sea ice filled outlet of Crane. The

https://doi.org/10.5194/egusphere-2024-1499
Preprint. Discussion started: 1 July 2024


REMA strip DEMs are referenced to the WGS64 ellipsoid and were corrected for the geoid using values from BedMachine (Morlighem, 2022; Morlighem et al., 2020) interpolated at each nodal point of our model domain.

The bedrock elevation was defined using the Huss and Farinotti (2014) bedrock DEM, who used a mass continuity approach informed by NASA's Operation IceBridge and ground based measurements to define a bedrock dataset across the Antarctic Peninsula at 100 m resolution. This dataset was merged with multibeam swath bathymetry data (Rebesco et al., 2014) which provided direct measurements of bedrock elevations in the vicinity of Crane's outlet and grounding line. However, due to uncertainty in the bedrock profile and recent observations suggesting that Crane's grounding line lay further downstream prior to the sea ice disintegration (Wallis et al., 2024), we performed an additional sensitivity experiment considering the shallower Bedmachine bed elevation data (Morlighem, 2022; Morlighem et al., 2020) to ensure that our conclusions would not be impacted by uncertainty in the estimated bed topography (Fig. S4).

The grounding line location and ice thicknesses across regions of floating ice were calculated from the floatation criterion considering the input surface and bedrock elevations and using uniform ice and ocean densities of 917kg $m^{-3}$ and 1030kg $m^{-3}$ respectively.

Monthly averaged ice velocity maps at 200 m grid spacing were derived from successive Sentinel-1 IW SLC image pairs (2014-2023) using a combination of coherent and incoherent offset tracking techniques (ENVEO et al., 2021; Nagler et al., 2021, 2015).

## 3 Methodology

### 3.1 Experiment Design

We performed a series of numerical simulations to quantify the buttressing resistance provided to Crane Glacier by the sea ice. The simulations were performed in two steps, an overview of which is given below with further details described in the following subsections.

In the first step, the rate factor, $A$ in Glen's flow law, was estimated through inversion of measured velocities, allowing us to reconstruct the stress field throughout Crane and the ambient sea ice. We used satellite imagery to extract the location of the calving front prior to the sea ice disintegration and calculated the normal resistive stress at these coordinates in order to quantify the buttressing effect of the sea ice. We made the same calculations at the location of the terminus in the days immediately after the sea ice disintegration and again at locations that the ice-front had retreated to in the following months (Table 1). We calculated the resistive stresses at these different locations in order to give context to the buttressing strength of the sea ice and melange plume downstream of Crane's terminus, with that provided by increasing sections of Crane's floating ice shelf in accordance with calving events in the months following the sea ice disintegration.

In the second step, we investigated the expected change in the near terminus stress regime following the loss of buttressing sea ice. After having inverted for $A$ and ensured that modelled ice velocities were in good agreement with observations, we perturbed the model in a diagnostic simulation by removing the sea ice from the domain and assessed the instantaneous change in stress regime.

https://doi.org/10.5194/egusphere-2024-1499
Preprint. Discussion started: 1 July 2024


**Table 1.** The terminus ID's referred to throughout the study represent the terminus locations extracted from satellite imagery with acquisition dates shown below. LandSat imagery was obtained courtesy of the U.S. Geological Survey

| Terminus ID | Date of Acquisition | Satellite |
|---|---|---|
| December 2021 | 13/12/2021 | LandSat 9 |
| January 2022 | 21/01/2022 | LandSat 9 |
| February 2022 | 24/02/2022 | LandSat 8 |
| March 2022 | 19/03/2022 | LandSat 9 |

### 3.2 Model Setup

We used the ice-flow model, Úa (Gudmundsson, 2020), which solves the governing equations of ice dynamics using the SSA approximation (Morland, 1987; MacAyeal, 1989). The model uses a 2D vertically integrated approach which allowed us to assess the stress distribution throughout the domain in lateral and transverse directions, enabling an investigation into the buttressing effects of the sea ice where effects of lateral drag from the margins of the fjord are captured.

The model domain included the entirety of Crane, along with all in-flowing tributary regions of the glacier and extended downstream from the outlet of Crane's fjord (Figure 1). The location of rock outcrops were defined using Landsat imagery and holes in the mesh were placed at these locations where areas of thin ice and high strain rates may have caused numerical difficulties for the ice flow model (De Rydt et al., 2015). Boundary conditions at the edges of the domain were fixed to ice flow velocities from observational data (ENVEO et al., 2021). A zero flow condition was imposed at the interior boundaries.

The finite element mesh was refined to a minimum resolution of 100 m over areas of sea ice and regions close to the terminus and grounding line positions of the glacier. To reduce computational cost, a coarser resolution was employed further upstream and varied based on flow velocities up to a maximum resolution of 2.5 km. A total of 36268 elements with mean size of 194.2 m made up the model domain.

### 3.3 Inversion

Model parameters for basal slipperiness ($C$) and ice rheology (rate factor, $A$) were determined through an inversion process (MacAyeal, 1993) based on ice velocity measurements following a commonly used methodology (e.g. Hill et al., 2018; Barnes et al., 2020; Sun and Gudmundsson, 2023). Ice rheology is assumed to follow Glen's Flow Law (Glen, 1955) with stress exponent, $n = 3$, and basal sliding is assumed to follow Weertman's sliding law (Weertman, 1957), with stress exponent, $m = 3$.

Prior values for A and C were chosen based on assumed temperature and flow velocity respectively, before iteratively updating these values to minimize the cost function, $J = I + R$. Here, $I$, represents the misfit between modelled and observed velocities and, $R$, is a regularization parameter. We used Tikhonov regularisation and performed L-curve analysis (Hansen, 1992) to optimize the regularization parameters, iterating until convergence.

https://doi.org/10.5194/egusphere-2024-1499
Preprint. Discussion started: 1 July 2024


The inversion was based on monthly averaged velocity measurements from November 2021. This negated the possibility of including any contamination which may be present in the January 2022 dataset which partly accounts for time periods both prior to and following the sea ice disintegration. Monthly averaged velocities from December 2021 were discounted due to high errors associated with the velocity measurements downstream of the terminus location, however sensitivity results show the choice of velocity dataset has little impact on the findings of the study (Fig. S6).

### 3.4 Diagnostic Modelling

After having inverted for $A$ and ensured that modelled ice velocities were in good agreement with observations, we performed a diagnostic simulation in order to assess the instantaneous change in the near-terminus stress regime following the loss of the sea ice. We perturbed the model by removing all ice from the model domain downstream of the December 2021 terminus location (Table 1). It is noted that for numerical reasons, removing the sea ice actually involves replacing the defined thickness with a nominal 0.1 m thickness, which is suitably thin so as not to impact the upstream flow of ice.

Prior to running the diagnostic simulation, the boundary conditions at the domain's flow outlet were changed to a stress-free condition.

### 3.5 Buttressing Quantification

Buttressing is commonly quantified by determining the normal resistive stress imparted by an ice shelf at the grounding line, $R_N$, and comparing this to the hypothetical ocean pressure which would be exerted at the same location in the absence of an ice shelf, $R_o$ (Schoof, 2007; Gudmundsson, 2013). Here we apply the same methodology, instead considering the normal resistive stress at the terminus.

$$R_o = \frac{1}{2}\rho_i \left(1 - \frac{\rho_i}{\rho_o}\right) gh \tag{1}$$

$$R_N = \boldsymbol{n}^\intercal \cdot (\boldsymbol{R}\boldsymbol{n}) \tag{2}$$

$$R = \begin{bmatrix} 2\tau_{xx} + \tau_{yy} & \tau_{xy} \\ \tau_{xy} & 2\tau_{yy} + \tau_{xx} \end{bmatrix} \tag{3}$$

where $g$ is the gravitational constant, $h$ is ice thickness, $(\boldsymbol{n})$ is the unit vector normal to the terminus, $R$ is the resistive stress tensor and $\tau_{ij}$ are components of the deviatoric stress tensor computed in the model inversion. Values of 917kg m$^{-3}$ and 1030kg m$^{-3}$ are considered for ice density, $\rho_i$, and sea water density, $\rho_o$, respectively.

The buttressing ratio is given by $\Theta_N$,

$$\Theta_N = \frac{R_N}{R_o} \tag{4}$$

https://doi.org/10.5194/egusphere-2024-1499
Preprint. Discussion started: 1 July 2024


The scenario of no buttressing is given by $\Theta_N = 1$, as the resistive stress imparted by the sea ice normal to the terminus is equal to that of the vertically integrated ocean pressure at the same location. $\Theta_N < 1$ shows there is a buttressing effect resisting ice flow, with decreasing values corresponding to increasing resistive stress. Where $\Theta_N > 1$, resistive stresses are less than in the hypothetical ice free scenario, indicating that ice is being pulled downstream. Where $\Theta_N < 0$, deviatoric stress normal to the terminus is compressive, otherwise it is tensile.

### 3.6 Sea Ice Thickness Sensitivity

The inversion process provides an optimised estimate of the ice rheology over both glacier and sea ice areas of the model domain. Crucially, this process accounts for the discontinuous nature of the sea ice and melange by returning a varied $A$ (rate factor) field, derived from the measured velocities and dependent upon the input ice thicknesses by solving the conservation of momentum equations with SSA approximation,

$$\partial_x(h(2\tau_{xx} + \tau_{yy})) + \partial_y(h\tau_{xy}) - t_{bx} = \rho_i g h \partial_x s \tag{5}$$

$$\partial_y(h(2\tau_{xx} + \tau_{yy})) + \partial_x(h\tau_{xy}) - t_{by} = \rho_i g h \partial_y s \tag{6}$$

where $h$ is ice thickness, $t_{bh}$ is the horizontal components of the basal stress vector (equal to zero in floating regions), $\rho_i$ is ice density, $g$ is the gravitational constant, $s$ is the ice surface elevation and $\tau_{ij}$ are components of the deviatoric stress tensor calculated using Glen's Flow Law,

$$\dot{\varepsilon}_{ij} = A\tau^{n-1}\tau_{ij} \tag{7}$$

where $\dot{\varepsilon}_{ij}$ are components of the strain rate tensor, $A$ is the rate factor, $\tau$ is the second invariant of the deviatoric stress tensor, $\tau_{ij}$, and $n$ is the stress exponent.

The product of rate factor and ice thickness are found in the left-hand side of the momentum equations (Eqns. 5 and 6), with ice thickness only appearing separately from the rate factor in the body force component on the right-hand side of the equations. We therefore tested the hypothesis that uncertainty in sea ice thickness measurements are accounted for in the inversion, as the resulting ice rheology is described not solely by the rate factor, rather by the product of $A \cdot h$.

We performed a series of sensitivity experiments by adjusting the prescribed surface elevation of sea ice and melange elements downstream of the December 2021 terminus in increments of $\pm 10\%$ up to a maximum $40\%$ change from the original surface elevations (Howat et al., 2019). In regions of thin sea ice, the minimum defined surface elevation was limited to 0.1 m.

We updated the model inversion for each new sea ice thickness configuration and using the newly optimised $A$ fields, we calculated the buttressing number at the terminus location in each sensitivity case. Our hypothesis would be proven if the calculated buttressing numbers were not affected by the adjustment in the input sea ice surface elevation.

https://doi.org/10.5194/egusphere-2024-1499
Preprint. Discussion started: 1 July 2024


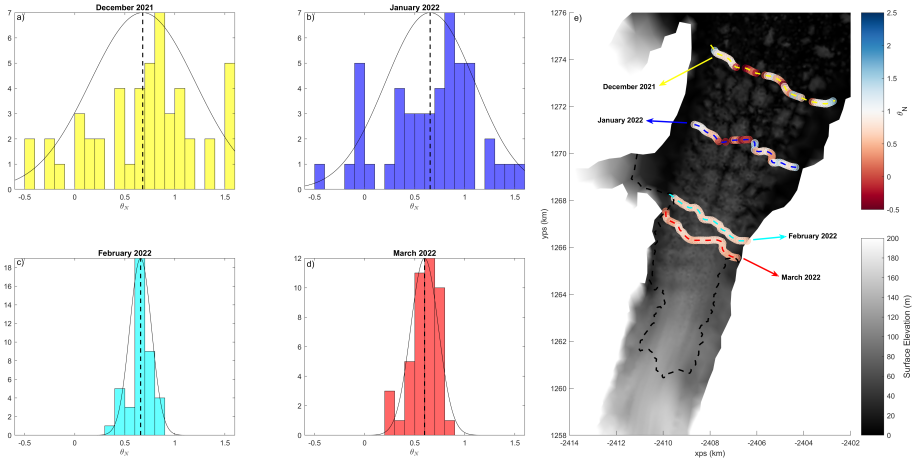


**Figure 3.** The buttressing ratio ($\Theta_N$, Eqn. 4) was defined at 100 m intervals along terminus positions derived from Landsat imagery representing the ice front in December 2021, January 2022, February 2022 and March 2022. Histograms of the buttressing ratios at these intervals for each month's terminus position are shown in panels a) - d) with a normally distributed probability density function overlain in black. The vertical black dotted line shows the mean buttressing ratio. Panel e) shows the buttressing numbers in coloured bubbles along the terminus location with yellow, blue, cyan and red dotted lines showing the terminus location in December 2021, January 2022, February 2022 and March 2022 respectively plotted on top of a surface elevation map of Crane's outlet region. The dotted black line shows the grounding line.

## 4 Results

### 4.1 Buttressing Number

High spatial variability in the calculated buttressing numbers are seen at the December 2021 and January 2022 terminus positions (Figure 3). Compression is seen in the central regions (red bubbles, Figure 3) and the majority of buttressing numbers lie below 1, showing that resistive backstresses are imparted by the sea ice and melange. Buttressing ratios exceed 1 in some cases close to the edges of the fjord indicating that ice at the margins is being pulled downstream. Mean buttressing ratios of 0.68 and 0.65 were found across the December 2021 and January 2022 terminus locations respectively with values between 0.8 and 0.9 occurring most frequently along these ice fronts.

The February 2022 and March 2022 terminus positions show a more consistent grouping of buttressing numbers with the majority of calculated $\Theta_N$ values lying between 0.6 and 0.7 (Figure 3). Buttressing ratios do not exceed 1 at any point with mean values of 0.66 and 0.60 calculated along the February 2022 and March 2022 ice-fronts respectively.

### 4.2 Change in Terminus Stress Regime

We compared Crane's stress regime from our inversion, representing the stress field in the glacier with sea ice still intact, against that from the diagnostic simulation in which sea ice was removed downstream of the December 2021 terminus. The removal of sea ice from the domain lead to an increase in extensional stresses running perpendicular to the ice front over the

https://doi.org/10.5194/egusphere-2024-1499
Preprint. Discussion started: 1 July 2024


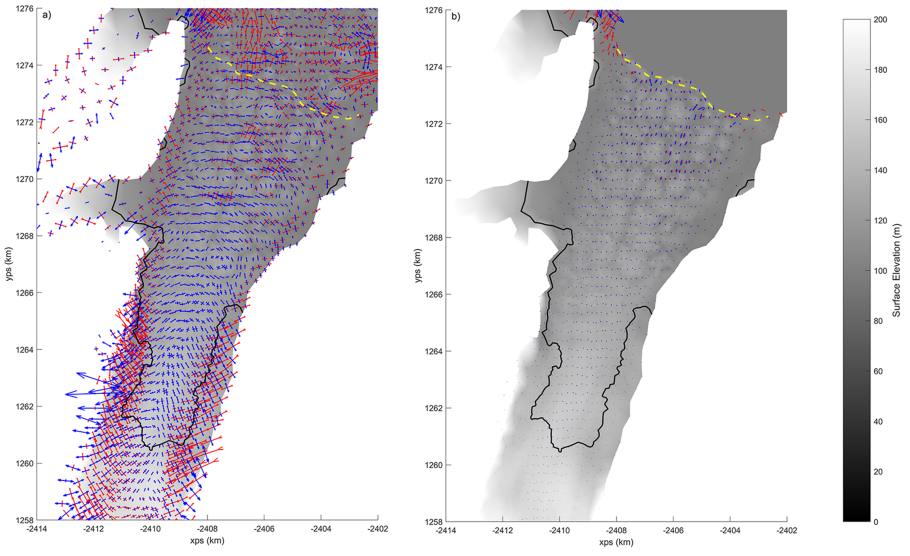


**Figure 4.** Extensional (blue) and compressive (red) principle stresses in the near-terminus region of Crane. The left hand plot shows the absolute stresses in the model configuration with sea ice intact. The right hand plot shows the change in stress distribution following the removal of sea ice downstream of the December 2021 terminus. Blue arrows in these plots represent an increase in extensional stresses. The yellow and black dotted lines represent the terminus and grounding line positions respectively. Maximum and mean increases in the 1st principle stress at the terminus are 70.8kPa and 19.2kPa respectively.

region of floating ice (Fig. 4). The magnitude of this change increased with closer proximity to the ice front where maximum and mean modelled increases in extensional stresses were found to be 70.8 kPa and 19.2 kPa respectively.

### 4.3 Sensitivity of Results to Sea Ice Thickness Definition

The buttressing numbers calculated across the terminus remain consistent across each sensitivity experiment with the spatial distribution of areas of high and low buttressing unchanged by the input ice thickness (Fig. 5). Greater resistive stresses are seen in the central region of the ice-front with areas of negative buttressing ($\Theta_N > 1$) seen at the margins.

A 14.3% increase in the mean value of $\Theta_N$ was calculated with ice thicknesses downstream of the terminus location reduced by 40% (the thinnest thickness distribution assessed). In all other sensitivity experiments, the mean value of $\Theta_N$ differed by a maximum of 6.6% from the reference configuration. No correlation between the percentage change in modelled thickness of sea ice and the deviation of mean buttressing number from the reference case results is observed. Uncertainty in the sea ice thickness profile therefore does not significantly affect our results.

https://doi.org/10.5194/egusphere-2024-1499
Preprint. Discussion started: 1 July 2024


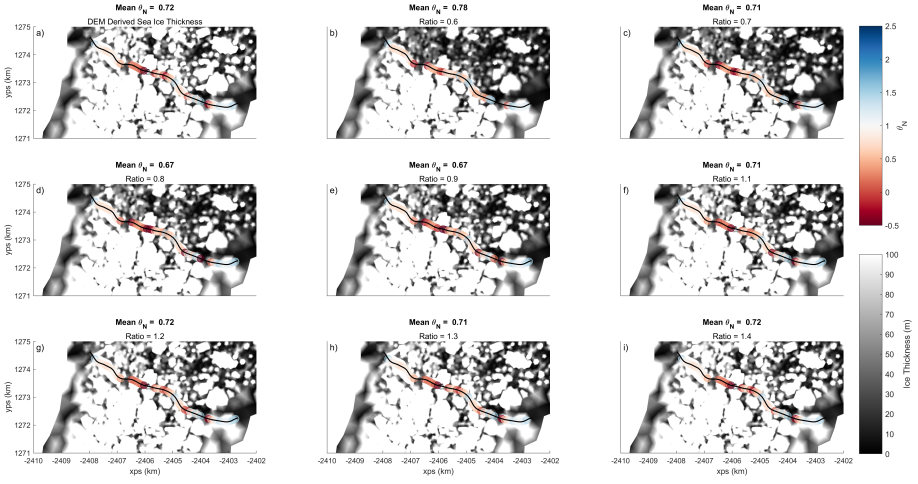


**Figure 5.** The buttressing numbers calculated at the December 2021 terminus location with sea ice represented by varying ice thicknesses in the model. Updated model inversions were performed separately for each configuration. In panel a), the sea ice and melange thicknesses downstream of the terminus were defined using the REMA strip DEMs as per the initial intact model configuration. In panels b) - i) Ice thicknesses downstream of the terminus were adjusted from the DEM derived thickness by the ratio displayed on each panel. The dashed yellow line shows the terminus location with buttressing numbers along this line shown by coloured bubbles at 100 m intervals.

## 5 Discussion

### 5.1 Buttressing Contribution of Sea Ice

As past studies sought to assess the role that sea ice plays in buttressing glaciers through interpretation of observational data (Sun et al., 2023; Ochwat et al., 2024), we sought to quantify this buttressing contribution for the first time using numerical modelling. With a mean buttressing number of 0.68 calculated at the interface between glacier and sea ice (Fig. 3), our results show that the sea ice provided significant resistive backstress to the glacier.

Negative buttressing numbers, which correspond to areas of compressive stress, were found in some locations across the December 2021 and January 2022 ice fronts (Fig. 3). Examination of satellite imagery (Fig. 2) and the surface elevation profile of the terminus region (Howat et al., 2019) highlights the discontinuous nature of the damaged ice shelf and melange in the transition between glacier and sea ice. Fragments of calved icebergs were also trapped by the sea ice, preventing transport away from the terminus and making the definition of an exact terminus location difficult to achieve. When we consider that the model reduces the resolution over this region of high variability in ice thickness to a 100 m grid, we anticipate that compression is found in regions of the model which are influenced by crevassing and fragmentation of the ice. These areas are unlikely to impart such high resistive stresses as the corresponding buttressing numbers suggest, which would result in the mean ratios being artificially shifted to a lower amount. If we instead consider the mode values calculated across the December 2021 and January 2022 terminus locations, we find buttressing numbers between 0.8 and 0.9 (Fig. 3). These values may therefore be more

https://doi.org/10.5194/egusphere-2024-1499
Preprint. Discussion started: 1 July 2024


representative of the buttressing strength of the sea ice than the mean values reported above. However, we can still conclude from this that buttressing was imparted by the sea ice prior to its disintegration and that the buttressing strength is lower than that provided by the ice shelf further upstream.

### 5.2 Crane's Response to Loss of Buttressing Sea Ice

The quantification of the buttressing contribution of both the sea ice and melange and the floating ice shelf (Fig. 3) provides insight into the observed response of Crane to the disintegration of Larsen B's landfast sea ice. Observational data shows 1) an acceleration of ice flow speed and 2) rapid calving of Crane's floating ice shelf.

The flow speed at the terminus increased by an average of 3.4% in the first month following the sea ice disintegration compared to when the sea ice was intact (Movie S2). A smaller increase of 0.5% across the grounding line was observed over the same time period. A fluctuation between increase and decrease in flow speed across the grounding line was observed until August 2022 with average flow speeds typically within 1% of the pre-disintegration velocities, however acceleration at the terminus region reached a maximum of 13.6% over this period, suggesting that the mechanical support supplied to the glacier by the sea ice played a greater role in restriction of ice flow at the terminus than further upstream at the grounding line.

Eight months later, in September 2022, increases in flow speed at the terminus and grounding line locations had increased to 14.10% and 7.54% respectively, with further increases observed in the following months (Fig. 2, Movie S2). Sun et al. (2023) argued that such a delay in the velocity response was due to the retreat of Crane's ice front, rather than being directly due to the collapse of the sea ice. However, our results suggest that these phenomena are connected and ultimately caused by the sea ice disintegration.

Satellite imagery showed Crane's terminus retreating by 6 km in the first month following the disintegration event (Fig. 2), with iceberg calving known to be triggered by changes in the state and integrity of adjoining sea ice (Christie et al., 2022; Arthur et al., 2021; Miles et al., 2017). Following the removal of the buttressing sea ice and melange from our model domain, an increase in extensional stresses was found in the vicinity of the terminus (Fig. 4), likely playing a key role in the initial calving response (Benn et al., 2007; Walter et al., 2010). It is noted that calving may have occurred more readily at this time as the near-terminus area was characterised by susceptible, highly damaged ice (Fig. 2), similar to observations reported by Amundson et al. (2010). A further assessment into the changes in stress regime following calving of the floating ice would be required to better understand the progressive calving behaviour seen later in the year.

As Crane's floating ice shelf also provided buttressing against upstream ice flow (Fig. 3), it follows that with each subsequent calving event, further resistive backstress was lost, ultimately leading to further acceleration of ice flow. With changes in grounding line flux most sensitive to loss of buttressing close to the location of the grounding line (Mitcham et al., 2022), we attribute any perceived delayed response in ice flow acceleration to be part of the evolving dynamic response of Crane following the loss of buttressing sea ice.

https://doi.org/10.5194/egusphere-2024-1499
Preprint. Discussion started: 1 July 2024


### 5.3 Sea Ice Thickness Definition

We configured the thickness of sea ice in our model using a high resolution surface elevation profile (Howat et al., 2019), defined at 2m resolution with an associated 2m error estimate per pixel. The average surface elevation of model elements downstream of the December 2021 terminus location is 4.57 m (41.66m thickness). If it is assumed that the maximum associated error of 2m exists over the entire modelled area of sea ice, the upper limit to the average change in surface elevation in this area is 43.75%.

The thinnest configuration of sea ice we tested considered a 40% reduction in surface elevation, which resulted in a 14.3% increase in the calculated mean buttressing ratio compared to the reference configuration (Fig. 5b). Results from the other sensitivity experiments were typically within about 6% of the reference configuration (Fig. 5). The amount by which these sensitivities deviated from the reference case was uncorrelated to the percentage change in surface elevation, showing that the rheology rate factor field, $A$, varied from case to case, thereby artificially correcting for any uncertainty in the input surface elevation of sea ice and melange.

Despite this variation in the exact distribution and magnitude of the modelled resistive stresses, the results from each sensitivity experiment point to the conclusion that the sea ice provided significant backstress to the glacier prior to its disintegration, with mean buttressing numbers at the glacier terminus between 0.67 and 0.72 in 7 out of the 8 sensitivity cases assessed, and below 0.8 in all sensitivity experiments.

## 6 Conclusions

We defined the stress regime in Crane glacier and the surrounding ambient sea ice through inverse modelling, allowing us to quantify the buttressing resistance provided to Crane by the sea ice for the first time.

Our results show that landfast sea ice over the Larsen B Embayment buttressed Crane prior to its disintegration in January 2022, with a mean buttressing number of 0.68 found at the interface between the glacier and the sea ice and melange mixture.

Observations showed a 3.4% increase in flow speed at the ice front and the rapid loss of 6 km of Crane's floating ice shelf in the first month after the disintegration, whilst our model simulations found a perturbation in the near-terminus stress regime following the loss of this buttressing sea ice. An average increase in extensional stresses normal to the terminus of 19.2 kPa likely triggered the rapid calving of Crane's floating ice over a region which was already highly damaged. The consequent loss of large portions of the floating ice shelf led to further reduction in resistive backstresses to the glacier, which was followed by further acceleration of ice flow throughout 2022.

The buttressing contribution of sea ice should therefore not be discounted from ice sheet modelling studies. We have shown that the stress distribution over regions of sea ice can be modelled effectively by considering the product of the rheology rate factor, $A$, optimised through inversion of measured velocities, and the input thickness of sea ice and melange, $h$. The product of $A \cdot h$ artificially corrects the optimised ice rheology, thereby accounting for uncertainties associated with sea ice thickness measurements. This methodology may therefore be considered as a way of accounting for backstresses imparted by regions of sea ice and melange.

https://doi.org/10.5194/egusphere-2024-1499
Preprint. Discussion started: 1 July 2024


*Code and data availability.* The open-source ice-flow model Úa used for the numerical simulations is preserved at https://doi.org/10.5281/zenodo.370662
Velocity data used in this study is available from Enveo's CryoPortal https://cryoportal.enveo.at/. LandSat-8 and LandSat-9 images were obtained courtesy of the U.S. Geological Survey from https://earthexplorer.usgs.gov/. The Reference Elevation Model of Antarctica strip DEMs were obtained from the Polar Geospatial Center Fridge web application, https://fridge.pgc.umn.edu/.

*Author contributions.* RP led the study, performed modelling work and processed results. SS and GHG initiated the study and contributed to discussion and interpretation of results. JW and TN provided monthly averaged ice flow velocity data for the study site. RP prepared the manuscript with contributions from all authors.

*Competing interests.* The authors declare that they have no conflict of interest.

*Acknowledgements.* Richard Parsons was supported by the National Environmental Research Council (NERC) funded ONE Planet Doctoral Training Partnership, hosted by Northumbria and Newcastle Universities. We acknowledge the use of datasets produced through the ESA project Antarctic Ice Sheet Climate Change Initiative (AIS CCI). G. Hilmar Gudmundsson was partially funded through grant NSFGEO-NERC:IceRift, NE/V013319/1.

https://doi.org/10.5194/egusphere-2024-1499
Preprint. Discussion started: 1 July 2024


## References

Amundson, J. M., Fahnestock, M., Truffer, M., Brown, J., Lüthi, M. P., and Motyka, R. J.: Ice mélange dynamics and implications for terminus stability, Jakobshavn Isbræ, Greenland, Journal of Geophysical Research: Earth Surface, 115, 2010.

Arthur, J. F., Stokes, C. R., Jamieson, S. S., Miles, B. W., Carr, J. R., and Leeson, A. A.: The triggers of the disaggregation of Voyeykov Ice Shelf (2007), Wilkes Land, East Antarctica, and its subsequent evolution, Journal of Glaciology, 67, 933–951, 2021.

Barnes, J. M., Dos Santos, T. D., Goldberg, D., Gudmundsson, G. H., Morlighem, M., and De Rydt, J.: The transferability of adjoint inversion products between different ice flow models, The Cryosphere Discussions, 2020, 1–32, 2020.

Benn, D. I., Warren, C. R., and Mottram, R. H.: Calving processes and the dynamics of calving glaciers, Earth-Science Reviews, 82, 143–179, 2007.

Christie, F. D., Benham, T. J., Batchelor, C. L., Rack, W., Montelli, A., and Dowdeswell, J. A.: Antarctic ice-shelf advance driven by anomalous atmospheric and sea-ice circulation, Nature Geoscience, 15, 356–362, 2022.

De Rydt, J., Gudmundsson, G., Rott, H., and Bamber, J. L.: Modeling the instantaneous response of glaciers after the collapse of the Larsen B Ice Shelf, Geophysical Research Letters, 42, 5355–5363, 2015.

ENVEO, Wuite, J., Hetzenecker, M., Nagler, T., and Scheiblauer, S.: ESA Antarctic Ice Sheet Climate Change Initiative (Antarctic Ice Sheet cci), Antarctic Ice Sheet monthly velocity from 2017 to 2020, derived from Sentinel-1, v1. NERC EDS Centre for Environmental Data Analysis, 28 June 2021, https://doi.org/10.5285/00fe090efc58446e8980992a617f632f, 2021.

Fogt, R. L., Sleinkofer, A. M., Raphael, M. N., and Handcock, M. S.: A regime shift in seasonal total Antarctic sea ice extent in the twentieth century, Nature Climate Change, 12, 54–62, 2022.

Fürst, J. J., Durand, G., Gillet-Chaulet, F., Tavard, L., Rankl, M., Braun, M., and Gagliardini, O.: The safety band of Antarctic ice shelves, Nature Climate Change, 6, 479–482, 2016.

Glen, J. W.: The creep of polycrystalline ice, Proceedings of the Royal Society of London. Series A. Mathematical and Physical Sciences, 228, 519–538, 1955.

Gomez-Fell, R., Rack, W., Purdie, H., and Marsh, O.: Parker Ice Tongue collapse, Antarctica, triggered by loss of stabilizing land-fast sea ice, Geophysical Research Letters, 49, e2021GL096 156, 2022.

Greene, C. A., Young, D. A., Gwyther, D. E., Galton-Fenzi, B. K., and Blankenship, D. D.: Seasonal dynamics of Totten Ice Shelf controlled by sea ice buttressing, The Cryosphere, 12, 2869–2882, 2018.

Gudmundsson, G.: Ice-shelf buttressing and the stability of marine ice sheets, The Cryosphere, 7, 647–655, 2013.

Gudmundsson, G.: GHilmarG/UaSource: Ua2019b (Version v2019b), https://doi.org/10.5281/zenodo.3706624, 2020.

Gudmundsson, G. H., Barnes, J. M., Goldberg, D., and Morlighem, M.: Limited impact of Thwaites Ice Shelf on future ice loss from Antarctica, Geophysical Research Letters, 50, e2023GL102 880, 2023.

Hansen, P. C.: Analysis of discrete ill-posed problems by means of the L-curve, SIAM review, 34, 561–580, 1992.

Hill, E. A., Gudmundsson, G. H., Carr, J. R., and Stokes, C. R.: Velocity response of Petermann Glacier, northwest Greenland, to past and future calving events, The Cryosphere, 12, 3907–3921, 2018.

Howat, I. M., Porter, C., Smith, B. E., Noh, M.-J., and Morin, P.: The reference elevation model of Antarctica, The Cryosphere, 13, 665–674, 2019.

Huss, M. and Farinotti, D.: A high-resolution bedrock map for the Antarctic Peninsula, The Cryosphere, 8, 1261–1273, 2014.

https://doi.org/10.5194/egusphere-2024-1499
Preprint. Discussion started: 1 July 2024


Liu, J., Zhu, Z., and Chen, D.: Lowest Antarctic sea ice record broken for the second year in a row, Ocean-Land-Atmosphere Research, 2, 0007, 2023.

MacAyeal, D. R.: Large-scale ice flow over a viscous basal sediment: Theory and application to ice stream B, Antarctica, Journal of Geophysical Research: Solid Earth, 94, 4071–4087, 1989.

MacAyeal, D. R.: A tutorial on the use of control methods in ice-sheet modeling, Journal of Glaciology, 39, 91–98, 1993.

Massom, R. A., Giles, A. B., Fricker, H. A., Warner, R. C., Legrésy, B., Hyland, G., Young, N., and Fraser, A. D.: Examining the interaction between multi-year landfast sea ice and the Mertz Glacier Tongue, East Antarctica: Another factor in ice sheet stability?, Journal of Geophysical Research: Oceans, 115, 2010.

Massom, R. A., Scambos, T. A., Bennetts, L. G., Reid, P., Squire, V. A., and Stammerjohn, S. E.: Antarctic ice shelf disintegration triggered by sea ice loss and ocean swell, Nature, 558, 383–389, 2018.

Miles, B. W., Stokes, C. R., and Jamieson, S. S.: Simultaneous disintegration of outlet glaciers in Porpoise Bay (Wilkes Land), East Antarctica, driven by sea ice break-up, The Cryosphere, 11, 427–442, 2017.

Mitcham, T., Gudmundsson, G. H., and Bamber, J. L.: The instantaneous impact of calving and thinning on the Larsen C Ice Shelf, The Cryosphere, 16, 883–901, 2022.

Morland, L.: Unconfined ice-shelf flow, Dynamics of the West Antarctic ice sheet, 4, 99–116, 1987.

Morlighem, M.: MEaSUREs BedMachine Antarctica, Version 3, https://doi.org/10.5067/FPSU0V1MWUB6, 2022.

Morlighem, M., Rignot, E., Binder, T., Blankenship, D., Drews, R., Eagles, G., Eisen, O., Ferraccioli, F., Forsberg, R., Fretwell, P., et al.: Deep glacial troughs and stabilizing ridges unveiled beneath the margins of the Antarctic Ice Sheet, Nature geoscience, 13, 132–137, 2020.

Nagler, T., Rott, H., Hetzenecker, M., Wuite, J., and Potin, P.: The Sentinel-1 mission: New opportunities for ice sheet observations, Remote Sensing, 7, 9371–9389, 2015.

Nagler, T., Wuite, J., Libert, L., Hetzenecker, M., Keuris, L., and Rott, H.: Continuous Monitoring of Ice Motion and Discharge of Antarctic and Greenland Ice Sheets and Outlet Glaciers by Sentinel-1 A B, in: 2021 IEEE International Geoscience and Remote Sensing Symposium IGARSS, pp. 1061–1064, https://doi.org/10.1109/IGARSS47720.2021.9553514, 2021.

Needell, C. and Holschuh, N.: Evaluating the Retreat, Arrest, and Regrowth of Crane Glacier Against Marine Ice Cliff Process Models, Geophysical Research Letters, 50, e2022GL102 400, 2023.

Ochwat, N. E., Scambos, T. A., Banwell, A. F., Anderson, R. S., Maclennan, M. L., Picard, G., Shates, J. A., Marinsek, S., Margonari, L., Truffer, M., et al.: Triggers of the 2022 Larsen B multi-year landfast sea ice breakout and initial glacier response, The Cryosphere, 18, 1709–1731, 2024.

Purich, A. and Doddridge, E. W.: Record low Antarctic sea ice coverage indicates a new sea ice state, Communications Earth & Environment, 4, 314, 2023.

Raphael, M. N. and Handcock, M. S.: A new record minimum for Antarctic sea ice, Nature Reviews Earth & Environment, 3, 215–216, 2022.

Rebesco, M., Domack, E., Zgur, F., Lavoie, C., Leventer, A., Brachfeld, S., Willmott, V., Halverson, G., Truffer, M., Scambos, T., et al.: Boundary condition of grounding lines prior to collapse, Larsen-B Ice Shelf, Antarctica, Science, 345, 1354–1358, 2014.

Reese, R., Gudmundsson, G. H., Levermann, A., and Winkelmann, R.: The far reach of ice-shelf thinning in Antarctica, Nature Climate Change, 8, 53–57, 2018.

Rignot, E., Casassa, G., Gogineni, P., Krabill, W., Rivera, A., and Thomas, R.: Accelerated ice discharge from the Antarctic Peninsula following the collapse of Larsen B Ice Shelf, Geophysical research letters, 31, 2004.

https://doi.org/10.5194/egusphere-2024-1499
Preprint. Discussion started: 1 July 2024


Robel, A. A.: Thinning sea ice weakens buttressing force of iceberg mélange and promotes calving, Nature Communications, 8, 14 596, 2017.

Rott, H., Abdel Jaber, W., Wuite, J., Scheiblauer, S., Floricioiu, D., Van Wessem, J. M., Nagler, T., Miranda, N., and Van Den Broeke, M. R.: Changing pattern of ice flow and mass balance for glaciers discharging into the Larsen A and B embayments, Antarctic Peninsula, 2011 to 2016, The Cryosphere, 12, 1273–1291, 2018.

Scambos, T., Moussavi, M., Abdalati, W., and Pettit, E.: Evolution of fast ice thickness from Cryosat-2 radar altimetry data, a case study in Scar Inlet, Antarctica, in: AGU fall meeting abstracts, vol. 2017, pp. C21G–1181, 2017.

Scambos, T. A., Bohlander, J., Shuman, C. A., and Skvarca, P.: Glacier acceleration and thinning after ice shelf collapse in the Larsen B Embayment, Antarctica, Geophysical Research Letters, 31, 2004.

Schoof, C.: Ice sheet grounding line dynamics: Steady states, stability, and hysteresis, Journal of Geophysical Research: Earth Surface, 112, 2007.

Sun, S. and Gudmundsson, G. H.: The speedup of Pine Island Ice Shelf between 2017 and 2020: revaluating the importance of ice damage, Journal of Glaciology, pp. 1–9, 2023.

Sun, Y., Riel, B., and Minchew, B.: Disintegration and Buttressing Effect of the Landfast Sea Ice in the Larsen B Embayment, Antarctic Peninsula, Geophysical Research Letters, 50, 2023.

Surawy-Stepney, T., Hogg, A. E., Cornford, S. L., Wallis, B. J., Davison, B. J., Selley, H. L., Slater, R. A., Lie, E. K., Jakob, L., Ridout, A., et al.: The effect of landfast sea ice buttressing on ice dynamic speedup in the Larsen B Embayment, Antarctica, The Cryosphere, 18, 977–993, 2024.

Teder, N., Bennetts, L., Reid, P., and Massom, R.: Sea ice-free corridors for large swell to reach Antarctic ice shelves, Environmental Research Letters, 17, 045 026, 2022.

Wallis, B. J., Hogg, A. E., Zhu, Y., and Hooper, A.: Change in grounding line location on the Antarctic Peninsula measured using a tidal motion offset correlation method, EGUsphere, 2024, 1–32, 2024.

Walter, F., O'Neel, S., McNamara, D., Pfeffer, W., Bassis, J. N., and Fricker, H. A.: Iceberg calving during transition from grounded to floating ice: Columbia Glacier, Alaska, Geophysical Research Letters, 37, 2010.

Weertman, J.: On the sliding of glaciers, Journal of glaciology, 3, 33–38, 1957.

Wuite, J., Rott, H., Hetzenecker, M., Floricioiu, D., De Rydt, J., Gudmundsson, G., Nagler, T., and Kern, M.: Evolution of surface velocities and ice discharge of Larsen B outlet glaciers from 1995 to 2013, The Cryosphere, 9, 957–969, 2015.